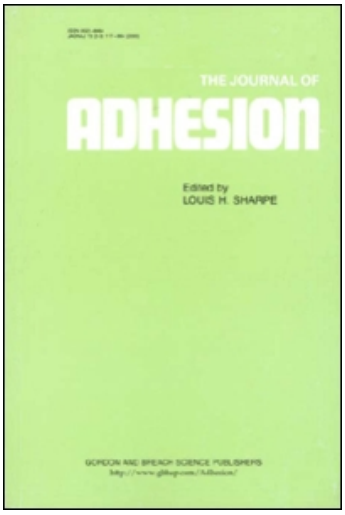

The Journal of Adhesion
Publication details, including instructions for authors and subscription information:
http://www.informaworld.com/smpp/title~content=t713453635

Closed Form Nonlinear Analysis of the Peninsula Blister Test

Dewei Xu[a]; Kenneth M. Liechti[a]; Thibault H. de Lumley-Woodyear[a]
[a] Research Center for the Mechanics of Solids Structures and Materials, Department of Aerospace Engineering and Engineering Mechanics, University of Texas at Austin, Austin, Texas, USA

To cite this Article Xu, Dewei , Liechti, Kenneth M. and de Lumley-Woodyear, Thibault H.(2006) 'Closed Form Nonlinear Analysis of the Peninsula Blister Test', The Journal of Adhesion, 82: 8, 831 — 866
To link to this Article: DOI: 10.1080/00218460600822922
URL: http://dx.doi.org/10.1080/00218460600822922

The Journal of Adhesion, 82:831–866, 2006

ISSN: 0021-8464 print/1545-5823 online
DOI: 10.1080/00218460600822922

Taylor & Francis
Taylor & Francis Group

Closed Form Nonlinear Analysis of the Peninsula Blister Test

Dewei Xu
Kenneth M. Liechti
Thibault H. de Lumley-Woodyear
Research Center for the Mechanics of Solids Structures and Materials, Department of Aerospace Engineering and Engineering Mechanics, University of Texas at Austin, Austin, Texas, USA

Previous work by Liechti and Shirani [1] has shown that, among the family of blister tests, the peninsula blister test is the best because of low plastic deformation. This work further examines the peninsula blister test, derives new solutions, and accounts for residual stresses. An approximate nonlinear analysis of the peninsula blister based on the minimum potential energy method was developed for extracting the toughness of thin films bonded to stiff substrates. This analysis, which is easily applied to specimens with finite dimensions, was validated against an exact analytical solution for plane strain and a three-dimensional finite element analysis. Experiments with a film adhesive, Hysol EA 9696®, were conducted. Bulge tests were used to obtain the elastic properties of and the residual stresses in the film. The fracture experiments were used to check the solutions and determine the toughness of the bond between the adhesive and aluminum. In both experiments, in addition to the usual measurements of volume and pressure, the deflection of the specimen was measured using shadow moiré. This allowed the residual stresses to be determined and their effects on both membrane deflection and energy release rate to be examined.

Keywords: Bulge test; Environmental effects; Ink jet printers; Microelectronics; Peninsula blister test; Residual stress; Thin film adhesion

Received 17 January 2006; in final form 22 May 2006.

Address correspondence to Kenneth M. Liechti, Aerospace Engineering and Engineering Mechanics, University of Texas, 210 East 24th Street, WRW 110C, 1 University Station, C0600, Austin, TX 78712-1085, USA. E-mail: kml@utexas.edu

1. INTRODUCTION

Thin film structures appear in a wide variety of applications such as functional and protective coatings, multilayer structures, and thin film/substrate structures in biological membranes, nanostructures, microelectronic devices and packages, reaction product layers, and adhesive joints. Interest in the measurement of thin film/substrate adhesion has increased with the development of microelectronic devices. A number of specialized techniques have been developed to measure adhesion in thin film/substrate structures where the thin films are sufficiently stiff with a relatively brittle interface. For example, in metal, oxide, or nitride films the scratch [2–5], peel and pull [6–8], four-point bending [9], stressed overlayers [10,11], indentation [12–14], and nanoindentation [15,16] tests were developed. A recent review [17] concluded that nanoindentation and stressed overlayers are by far the most common and reliable of these testing techniques.

For systems where one or both of the materials being joined are flexible, soft, and thin, plastic dissipation can play a key role in delamination. Peel tests [18,19] have been used for a long time to study the strength of adhesion of multilayer structures. However, they can produce a lot of plastic deformation, which may mask the determination of the actual fracture energy. Elastoplastic analyses [20–23] were conducted to account for the plastic dissipation. Pressurized blister tests were developed as an alternative, with the promise of lower plastic dissipation. The first blister test [24] was used to measure the adhesion of thick organic coatings to metals. A point-loaded configuration [25] was developed where a central point load was applied to the delaminating film, which resulted in outward radial growth of the crack. The work of adhesion was deduced by measuring the work done by the applied load. This configuration has recently been reintroduced in the form of the shaft-loaded blister [26]. A pressurized version of the blister test was first suggested by Williams [27] where pressurized circular blister specimens were used to establish that the adhesive fracture energy, represented by the critical energy release rate, is a system parameter that is independent of geometry. Pressurized circular blister specimens were used to explore [28] some aspects of surface interactions of polymers in thin film adhesion applications. Gent and Lewandowski [29] used membrane analysis to determine the onset and subsequent propagation of circular blisters under large deflections. Under pressure control, circular blister specimens are inherently unstable; *i.e.*, once a crack nucleates it will continue to grow. This instability can be avoided by conducting experiments under volume control. This

concept was used to advantage in high-temperature experiments [30,31] by using a fixed amount of the pressurizing medium.

Unfortunately, the critical pressure for crack initiation could not always be found because of bursting of thin, well-adhering delaminating layers [32]. As a result, the constrained blister test was proposed [33,34] to cope with this problem. The energy release rate can be selected by adjusting the height of the constraint, which enables the critical pressure and stress in the film to be deduced. The island blister [35] test was developed for the same reason. The drawback of the island blister test is that, under pressure control, the energy release rate increases with debond radius without bound, which induces unstable crack growth. To overcome this problem while maintaining a high energy release rate, which is the prerequisite for thin, well-adhering delaminating layers, Dillard and Bao [36] developed the peninsula blister test and showed that a constant energy release rate during debonding can be made to be very high.

The best configuration among all the blister tests is the one in which the amount of plastic dissipation is minimized so that the intrinsic adhesive fracture energy is extracted precisely. Liechti and Shirani [1] used nonlinear Von Karman plate theory to compare the circular, island, and peninsula blister specimens in a consistent manner. They showed that large-scale yielding occurs in all configurations except the case of relatively thick peninsula blister specimens. Lai and Dillard [37] introduced a fracture efficiency parameter to compare the abilities of different blister geometries to induce debonding without causing rupture of the film or yielding. They defined this parameter as the ratio between the energy release rate and the square of the maximum stress. If this parameter is to be at all useful for optimizing the specimen dimensions for a given blister geometry, it should take into account the extent of yielding within the film, rather than just the maximum value of stress. For example, large stresses might be produced and confined to a small region such as the vicinity of the crack front. In this case, the plastic zone is small, and an elastic analysis of the blister remains valid to compute the energy release rate. To account for global plastic dissipation within thin film blistering, Shirani and Liechti [38] adopted the fracture process zone model approach, proposed by Needleman [39,40]. This approach consists of attributing a traction-separation law to the interface and allows the plastic dissipation and adhesive fracture energy to be distinguished. Shirani and Liechti [41] showed that the amount of plastic dissipation was large for the circular blister specimen, whereas it was limited to a smaller region in the case of the peninsula blister. As a result, the latter configuration allows thin film adhesion to be determined from relatively simple elastic analyses.

The analyses just described involved plasticity and highly nonlinear traction-separation laws in sophisticated finite element analyses. They showed that an elastic analysis of the peninsula blister would suffice. Nonetheless, nonlinearities do arise when large deflections are needed to cause delamination. The purpose of the present study was to develop an accurate nonlinear analysis whose results are easily accessible to all users of the peninsula blister test.

2. EXPERIMENTAL

In this section, we describe the specimen fabrication and the apparatus used to conduct the bulge and peninsula blister experiments. The former was conducted after the latter and was used to determine the elastic properties of the film and the residual stress. The pressurized peninsula blister test was used to determine the adhesion of the film adhesive to an aluminum substrate.

2.1. Specimen Fabrication

The peninsula blister specimen is a rectangular blister configuration where the film is clamped along all four edges and bonded along a narrow long central strip, the "peninsula" (Figure 1). The widths of the peninsula and the specimen are $2b$ and $2c$, respectively, and l_0 is the initial debond length. It consists of three regions, region 2 and two regions 1, which together are called the "ocean." A Hysol EA 9696 film adhesive[1] (Henkel Loctite Corp., Rocky Hill, CT, USA) was bonded to an aluminum (6061-T6) substrate, whose surface was phosphoric acid anodized, and then coated with the BR® 127 (Cytec Fiberite, Havre de grace, MD, USA), a corrosion inhibiting primer that was cured at 100°C for 60 mins. A 25.4-μm cellophane tape (PCT-2A, Measurements group, Raleigh, NC, USA) was attached to the adhesive film with the nonstick surface facing the aluminum in order to provide a release layer and establish the initial debond length (region 2). The substrate was mounted on a Teflon® block that had been machined to form a mask in the ocean region. The Hysol EA 9696 film was deposited on both the treated substrate and Teflon mask and cured at 100°C for 90 min in an evacuated oven to reduce the formation of air bubbles. After curing the specimen, a thin layer of white paint was sprayed on the top of the adhesive for shadow moiré measurements.

[1]The authors gratefully acknowledge Loctite Aerospace for providing the EA 9696 gratis.

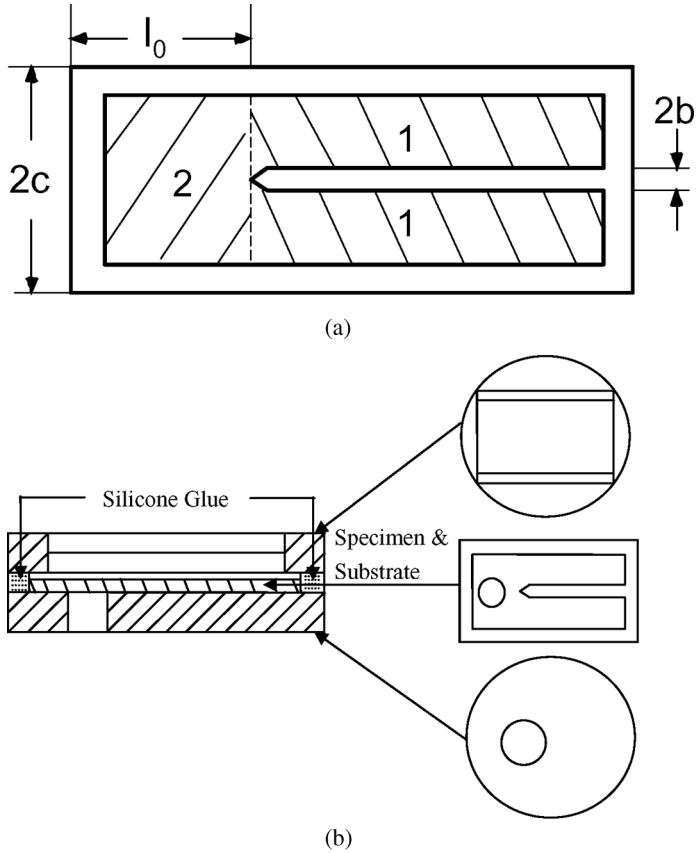

FIGURE 1 (a) Geometry and (b) mounting of the peninsula blister specimen.

2.2. Apparatus

A schematic view of the apparatus used in this study is shown in Figure 2. It consisted of a pressurization device along with data acquisition equipment and the components for shadow moiré, which was used to measure the deflected shape of the pressurized film. The specimen was placed between two circular plates and sealed in a manifold with silicone glue. The pressurizing medium was deionized water, and a syringe pump was used to control the flow rate. The pressure was measured with a pressure transducer (Sensotec Z/0761-09ZG, Honeywell Sensotec, Columbus, OH, USA) with a capacity of 344.7 kPa. It was connected to a data acquisition board (National Instruments PCI-MIO-16XE-50, National Instruments, Austin, TX,

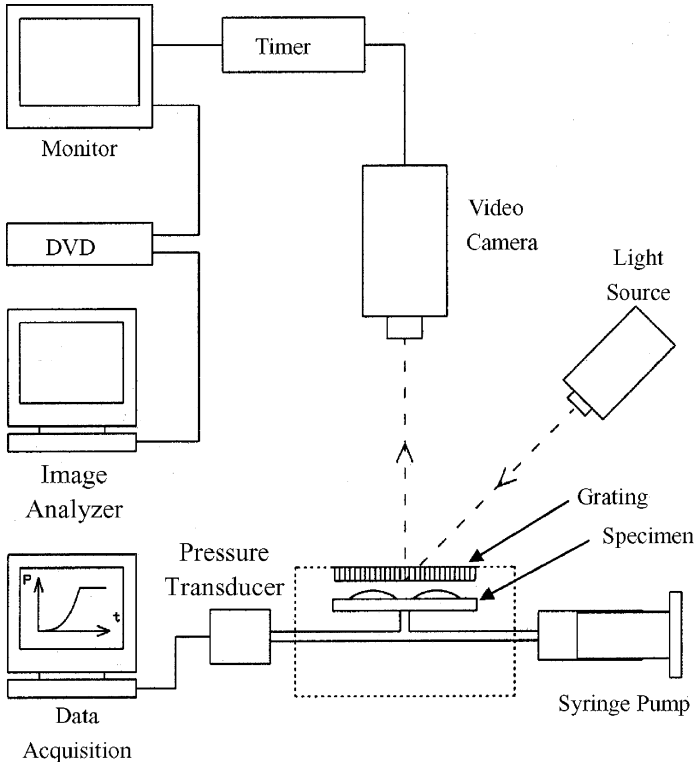

FIGURE 2 Schematic view of the apparatus.

USA), which was installed in a PC with LabVIEW software. The blister shape was measured using shadow moiré in which a master grating of 250 lines per inch was used, providing a half fringe resolution of 50.8 μm.

2.3. Bulge Test

The bulge test was conducted following the blister test to ensure that the material properties of the film adhesive were determined from the same material that was used in the blister test. The Young's modulus, E, and the residual stress, σ_0, can be extracted from the pressure-central deflection $(q - w_0)$ response by fitting (see Appendix B)

$$q = \frac{2h\sigma_0}{c^2} w_0 + \frac{8Eh}{6c^4(1-\nu^2)} w_0^3 \tag{1}$$

to the measured response. It can be seen that the initial slope of the response can be used to determine the residual stress in the film. The nonlinear term, on the other hand, yields information about Young's modulus. Poisson's ratio, ν, can be obtained [42] by conducting bulge tests on square and rectangular specimens. In this study, Poisson's ratio was set to 0.3 because its effect is small. The largest source of error in extracting Young's modulus is the uncertainty in specimen width, which enters as the fourth power. In the present study, fortunately, the dimension was readily determined as the width of the substrate.

Figure 3 shows the pressure-central deflection response of the pressurized film and two consistent loading cycles. The Young's modulus of, and the residual stress in, the film were 1.78 ± 0.02 GPa and 5.70 ± 0.03 MPa, respectively, based on Poisson's ratio of 0.30. The uncertainties were based on the uncertainty of measurements of the width of the substrate. Young's modulus of epoxy adhesives ranges from 1.0 to 3.0 GPa depending on curing temperature, pressure, composition, curing agent, modifiers, etc. The residual stresses were mainly caused by thermal contraction and can be estimated by

$$\sigma^R = \frac{E(\alpha_f - \alpha_s)}{1 - \nu}(T_c - T_a), \tag{2}$$

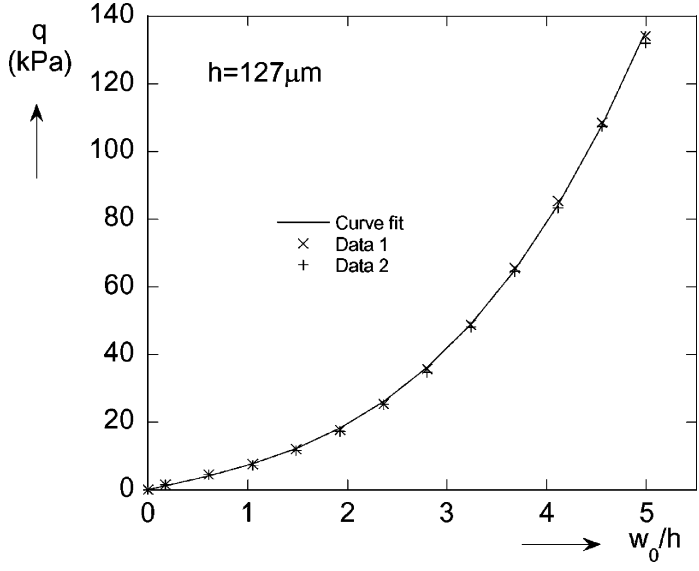

FIGURE 3 Measured pressure–normalized deflection response for a Hysol EA 9696 bulge specimen with an aspect ratio of 3.4.

where T_c is the stress-free cure temperature (100°C), T_a is the ambient temperature (25°C), and α_f and α_s are the coefficients of thermal expansion of the film and the substrate, respectively. For the adhesive film used in this study, α_f ranges from 50 to 60 μm/m/°C whereas α_s for the aluminum substrate is about 24 μm/m/°C. The resulting residual stress ranges from 4.96 MPa to 6.86 MPa, so the measured value 5.70 MPa of the residual stress seems to be reasonable.

2.4. The Peninsula Blister Test

After the peninsula specimen was fabricated, it was placed between two circular plates and sealed by silicone glue (Figure 1b). Then the assembly was fixed in the holder so that it could be pressurized. The initial crack length was set at an aspect ratio $l_0/2c$ of 1.5. The pumping rate was 5 ml/h, and Figure 4 shows typical pressure and debond length histories. Initially, the blister behaved as a membrane until debonding developed under increasing pressure. When the debonding initiated from the tip of the peninsula and the cellophane tape, which essentially formed a blunt crack, the pressure history reached a noticeable maximum before dropping to a nearly constant value. During this time the crack accelerated. However, once the

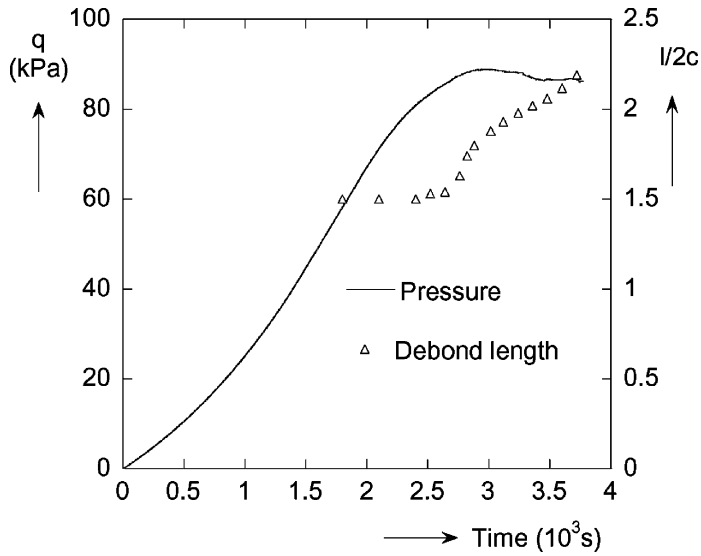

FIGURE 4 Typical pressure and debond length histories during a peninsula blister test with Hysol EA 9696 bonded to Al 6061-T6.

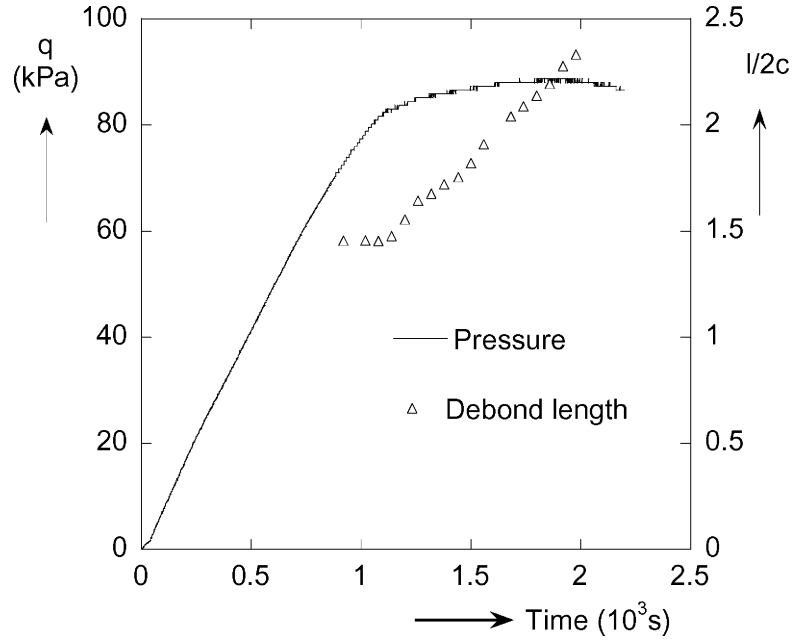

FIGURE 5 Pressure and debond length histories during a peninsula blister test with Hysol EA 9696 bonded to Al 6061-T6, starting from a sharp initial debond.

pressure became constant, the crack speed became steady. This constant pressure level was then used to determine the energy release rate at the steady state crack speed. The pressure history was slightly different (Figure 5) when the specimen was unloaded from the steady state response and then reloaded. There was an obvious discontinuity associated with the initiation of the crack, followed by an increase in pressure until the crack sensed the presence of the boundary. The rise in pressure could be associated with resistance curve effects. However, the increase in pressure was less than 2%.

3. ANALYSES

In this section, we present analyses of the peninsula blister specimen. Its geometry is presented first, followed by the analyses of a fully clamped membrane and the effects of residual stresses. These results are then used to derive the energy release rate.

3.1. The Peninsula Blister Specimen

As mentioned, the peninsula specimen consists of three separate regions. Each one can be thought of as a membrane clamped on three boundaries. The fourth boundary of each membrane is in the transition region identified by the delamination front on the peninsula. Debonding starts at the peninsula tip and propagates along the peninsula. In so doing, region 2 becomes larger at the expense of regions 1 on either side of the peninsula, with concomitant changes in stresses, strains, and potential energy. As debonding progresses, the size of the crack front remains constant and equal to the width of the peninsula.

3.2. Fully Clamped Membrane

The first step that was taken was to examine the response of fully clamped rectangular membranes (Figure 6) analytically. A closed-form solution completely satisfying the equilibrium equations and boundary conditions for nonlinear rectangular membranes is not possible. Thus, either an approximate analytical solution or a numerical solution can be pursued.

Membrane behavior arises when the deflection, w, is much greater than the thickness, h. If u and v are the in-plane displacements of the membrane associated with the x and y directions, respectively, the strains in the membrane are given by

$$\varepsilon_x = \frac{\partial u}{\partial x} + \frac{1}{2}\left(\frac{\partial w}{\partial x}\right)^2,$$
$$\varepsilon_y = \frac{\partial v}{\partial y} + \frac{1}{2}\left(\frac{\partial w}{\partial y}\right)^2, \tag{3}$$

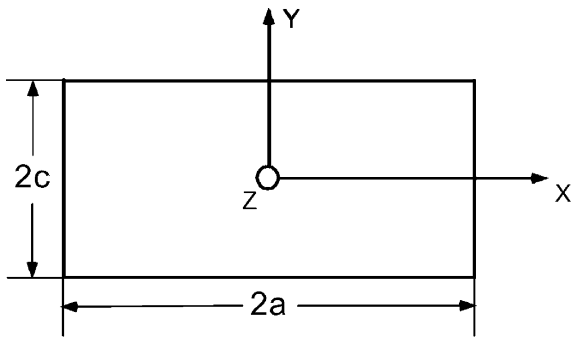

FIGURE 6 Rectangular membrane geometry.

and

$$\gamma_{xy} = \frac{\partial u}{\partial y} + \frac{\partial v}{\partial x} + \frac{\partial w}{\partial x}\frac{\partial w}{\partial y}.$$

The nonlinear terms in these expressions arise from the fact that the deflection of the membrane in the z direction is large. In the present study, an energy minimization approach was used where an approximate displacement field is employed. The most common approximate displacement field is the first term in the Fourier expansion of the actual deflection [43]. Such an approach was followed in analyses of the bulge test [42,43]. In the rectangular bulge tests that were conducted as a part of the present study, shadow moiré measurements of the film deflection verified that the slope near both the shorter clamped and at the longer clamped boundaries was finite. To determine the energy release rate, the whole deflection field is required. Such a deflection field cannot be properly represented by the first-order term used in previous analyses. Accordingly, we considered the following basis functions to describe the displacement field for a rectangular membrane

$$w = \left[1 - \left(\frac{x}{a}\right)^2\right]\left[1 - \left(\frac{y}{c}\right)^2\right]\sum_{i=1}^{N=5} w_{i-1}\left(\frac{x}{a}\right)^{2(i-1)}, \tag{4a}$$

$$u = u_0\left(\frac{x}{a}\right)\left[1 - \left(\frac{x}{a}\right)^2\right]\left[1 - \left(\frac{y}{c}\right)^2\right], \tag{4b}$$

and

$$v = v_0\left(\frac{y}{c}\right)\left[1 - \left(\frac{x}{a}\right)^2\right]\left[1 - \left(\frac{y}{c}\right)^2\right]. \tag{4c}$$

These functions vanish at the edges, thereby satisfying the boundary conditions imposed by clamped edges. Note that $\partial w/\partial y \neq 0$ at $y = \pm c$ and $\partial w/\partial x \neq 0$ at $x = \pm a$ corresponding to standard membrane behavior. This set of functions satisfies symmetry conditions: u and v are odd functions in x and y, respectively, and w is an even function in x and y. The first parenthesis term in w was taken to be a function of x only so as to account for the rectangular shape.

The parameters w_0, w_1, w_2, w_3, w_4 and u_0, v_0 were determined by minimizing the potential energy, Π, of the system through

$$\frac{\partial \Pi}{\partial w_0} = 0, \quad \frac{\partial \Pi}{\partial w_1} = 0, \quad \frac{\partial \Pi}{\partial w_2} = 0, \quad \frac{\partial \Pi}{\partial w_3} = 0, \quad \frac{\partial \Pi}{\partial w_4} = 0, \quad \frac{\partial \Pi}{\partial u_0} = 0, \quad \frac{\partial \Pi}{\partial v_0} = 0. \tag{5}$$

The potential energy is given by

$$\Pi = U - W, \tag{6}$$

where U is the strain energy of the film.

$$U = \frac{Eh}{2(1-\nu^2)} \iint \left[\varepsilon_x^2 + \varepsilon_y^2 + 2\nu\varepsilon_x\varepsilon_y + \frac{1}{2}(1-\nu)\gamma_{xy}^2 \right] dx\, dy, \tag{7}$$

where E, ν, and h are the Young's modulus, Poisson's ratio, and the thickness of the film, respectively.

The external work is given by

$$W = \iint qw\, dx\, dy, \tag{8}$$

where q is the uniform pressure on the film.

Minimization of the potential energy with respect to the undetermined parameters leads to a set of seven simultaneous nonlinear equations in w_0, w_1, w_2, w_3, w_4 and u_0, v_0 that were solved using Mathematica®.

The seven unknowns are given by

$$\begin{aligned}
w_0 &= f_1\left(v, \frac{a}{c}\right)\left(\frac{qc^4}{Eh}\right)^{1/3}, \\
w_1 &= f_2\left(v, \frac{a}{c}\right)\left(\frac{qc^4}{Eh}\right)^{1/3}, \\
w_2 &= f_3\left(v, \frac{a}{c}\right)\left(\frac{qc^4}{Eh}\right)^{1/3}, \\
w_3 &= f_4\left(v, \frac{a}{c}\right)\left(\frac{qc^4}{Eh}\right)^{1/3}, \\
w_4 &= f_5\left(v, \frac{a}{c}\right)\left(\frac{qc^4}{Eh}\right)^{1/3}, \\
u_0 &= f_6\left(v, \frac{a}{c}\right)\left(\frac{q^2c^5}{E^2h^2}\right)^{1/3}.
\end{aligned} \tag{9}$$

and

$$v_0 = f_7\left(v, \frac{a}{c}\right)\left(\frac{q^2c^5}{E^2h^2}\right)^{1/3}.$$

For an infinitely long membrane, the deflection will approach the plane strain solution given in Appendix A. In this case, an exact

solution for the membrane deflection and inplane displacement can be derived as

$$w = \sqrt[3]{\frac{6qc^4(1-\nu^2)}{8hE}}\left[1-\left(\frac{y}{c}\right)^2\right] \tag{10a}$$

and

$$v = \sqrt[3]{\frac{(1-\nu^2)^2q^2c^5}{6h^2E^2}}\left(\frac{y}{c}\right)\left[1-\left(\frac{y}{c}\right)^2\right]. \tag{10b}$$

The functions $f_1(\nu, a/c)$ and $f_7(\nu, a/c)$ in Eq. 9, will converge to $\sqrt[3]{6(1-\nu^2)/8}$ and $\sqrt[3]{(1-\nu^2)^2/6}$, respectively, when the aspect ratio a/c of the rectangle becomes large enough.

From Eq. (4), it can be seen that the dominant term is the one involving w_0. As a result, with reference to Eq. (9), it is instructive to examine the behavior (Figure 7) of the function $f_1(\nu, a/c)$. It can be seen that the deflection of a membrane increases rapidly for aspect ratios in the range $1 \leq a/c \leq 2$, but once the aspect ratio exceeds 3, the deflection is almost independent of the aspect ratio. The deflection is a weak function of Poisson's ratio. In fact, when the aspect ratio is larger

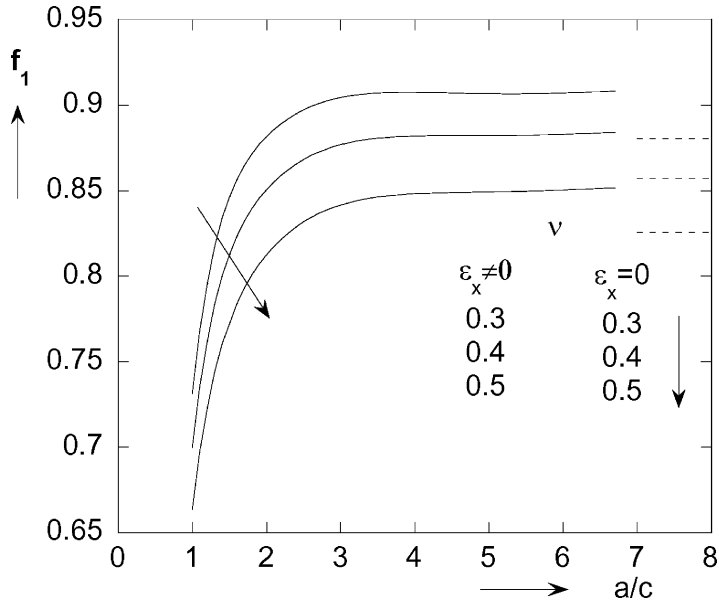

FIGURE 7 Variation of f_1 with aspect and Poisson's ratio.

than 2, the deviation from the plane strain solution is less than 3%. For each value of Poisson's ratio, the asymptote of $f_1(\nu, a/c)$ was larger than the plane strain solution. The reason for this is that for a rectangular membrane with a finite aspect ratio where the deflection varies with x, the maximum deflection, which $f_1(\nu, a/c)$ contributes to, should be larger than the plane strain solution to maintain the same energy. In subsequent analyses, we used the plane strain assumption when the aspect ratio was greater than 2.

Some remarks about the selection of the deflection functions are in order. First, it is indeed sufficient to select polynomials in x only in the series of the deflection function w. If polynomials in y are included, there is only a small effect. For example, compare the two sets of deflection functions

$$w = \left[w_0 + w_1\left(\frac{x}{a}\right)^2\right]\left[1 - \left(\frac{x}{a}\right)^2\right]\left[1 - \left(\frac{y}{c}\right)^2\right], \tag{11a}$$

or

$$w = \left[w_0 + w_1\left(\frac{x}{a}\right)^2 + w_2\left(\frac{y}{c}\right)^2\right]\left[1 - \left(\frac{x}{a}\right)^2\right]\left[1 - \left(\frac{y}{c}\right)^2\right] \tag{11b}$$

and

$$w = \left[w_0 + w_1\left(\frac{x}{a}\right)^2 + w_2\left(\frac{x}{a}\right)^4 + w_3\left(\frac{x}{a}\right)^6 + w_4\left(\frac{x}{a}\right)^8\right] \times \left[1 - \left(\frac{x}{a}\right)^2\right]\left[1 - \left(\frac{y}{c}\right)^2\right], \tag{12a}$$

or

$$w = \left[w_0 + w_1\left(\frac{x}{a}\right)^2 + w_2\left(\frac{x}{a}\right)^4 + w_3\left(\frac{x}{a}\right)^6 + w_4\left(\frac{x}{a}\right)^8 + w_5\left(\frac{y}{c}\right)^2\right] \times \left[1 - \left(\frac{x}{a}\right)^2\right]^2\left[1 - \left(\frac{y}{c}\right)^2\right]. \tag{12b}$$

Figure 8a is a comparison of f_1 as a function of aspect ratio with [Eq. (11b)] or without [Eq. (11a)] y terms, and Figure 8b is a similar comparison based on Eq. (12). Notice that y terms did not have much of an effect on f_1. The reason for this can be seen from the plane strain solution, where the term $1 - (y/c)^2$ is sufficient to characterize the deflection in the y direction.

Second, five terms in the series in Eq. (4a) are the fewest that are required to provide a satisfactory solution. Figure 9a shows the comparison of f_1 as a function of aspect ratio when the number

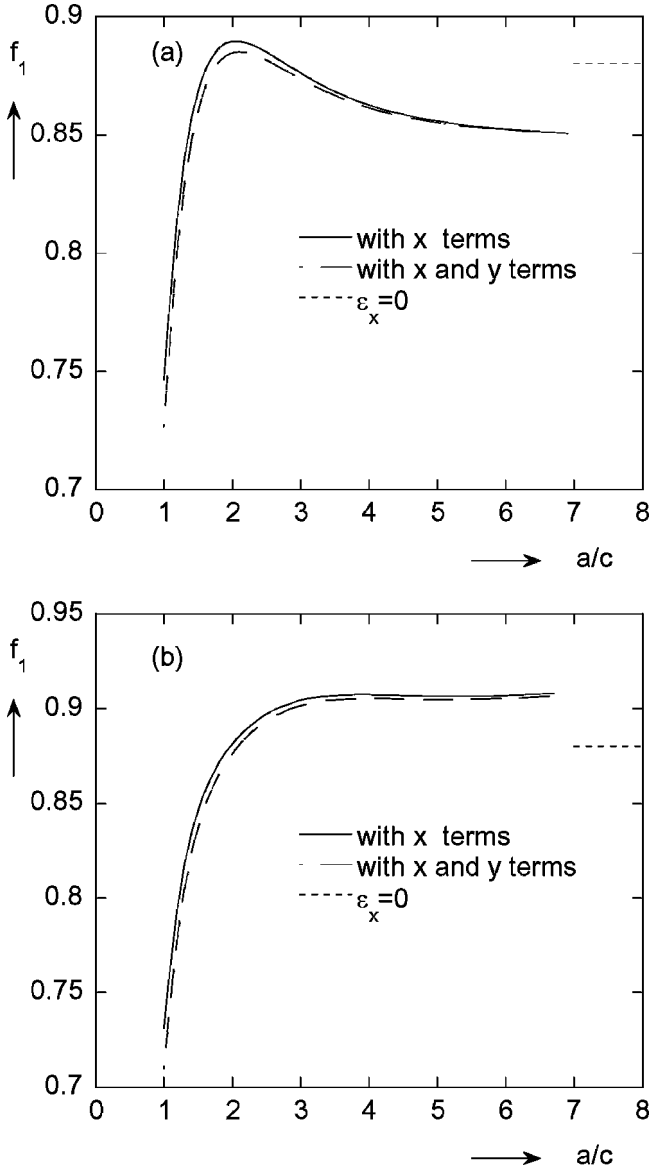

FIGURE 8 Variation of f_1 with aspect ratio with or without y terms in (a) Eqs. (9b) or (9a) and (b) Eqs. (10b) or (10a) ($\nu = 0.3$).

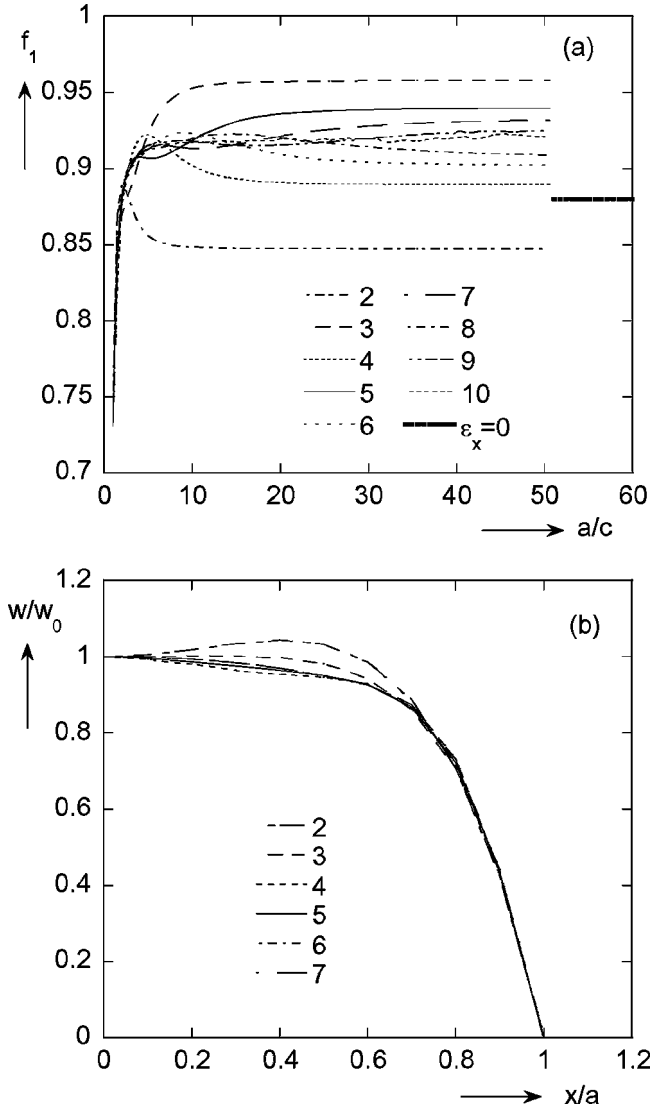

FIGURE 9 (a) Variation of f_1 with aspect ratio and number of degrees of freedom, and (b) the deflection along $y = 0$ for a membrane with an aspect ratio of 3.4 and $\nu = 0.3$.

of terms in the series varies from two to ten terms; *i.e.*, $2 \leq N \leq 10$. It is clear that each series approaches a different asymptote. However, as the number of terms increases, there is a convergence of asymptotic values with odd-numbered series approaching from above and

TABLE 1 Comparison of Asymptotes with Different Numbers of Terms

Parameter	2	3	4	5	6	7	8	9	10
$a/c = 50$	0.847	0.958	0.889	0.939	0.902	0.931	0.909	0.925	0.922
Deviation (%)	−8.13	3.83	−3.57	1.86	−2.18	0.99	−1.45	0.35	0

even-numbered series approaching from below. Notice that there were perturbations in f_1 as $N \geq 9$. The reason for this is that the error from the numerical analysis played a key role. If N is even, there will be a prominent maximum before approaching the asymptote. Vlassak and Nix [42], who used Eq. (11b), had noticed this feature and obtained a hump in f_1 for $a/c = 2$. Actually, as more terms are involved in the series, the prominent maximum becomes weaker and weaker, and finally disappears when $N \geq 10$. If N is odd, there will be a transition stage in f_1 before approaching the asymptote. Again, this transition stage disappeared when $N \geq 9$. The deviations of asymptotes as a function of the number of terms in the series are compared with the asymptote for ten terms in Table 1. When five terms were chosen, the deviation was less than 2%. Figure 9b shows the total deflection of the membrane along $y = 0$ for $2 \leq N \leq 7$. Note that when $N \geq 5$, the membrane shape did not change much. For consideration of both the convergence of f_1 and the whole deflection field of interest, the selection of five terms was considered to be sufficient.

2.3. The Influence of Residual Stresses on the Deflection of a Membrane

Until now, only membranes without residual stresses have been considered. The presence of such stresses, $\sigma_x^R$and σ_y^R, can alter the deflection behavior of a membrane and the strain energy release rate considerably [44]. The residual stresses can be included in the strain-displacement equations. That is,

$$\varepsilon_x = \frac{\partial u}{\partial x} + \frac{1}{2}\left(\frac{\partial w}{\partial x}\right)^2 + \frac{\sigma_x^R - \nu\sigma_y^R}{E},$$
$$\varepsilon_y = \frac{\partial v}{\partial y} + \frac{1}{2}\left(\frac{\partial w}{\partial y}\right)^2 + \frac{\sigma_y^R - \upsilon\sigma_x^R}{E}, \tag{13}$$

and

$$\gamma_{xy} = \frac{\partial u}{\partial y} + \frac{\partial v}{\partial x} + \frac{\partial w}{\partial x}\frac{\partial w}{\partial y}.$$

In thin film applications, the residual stresses might be due to thermal expansion effects, epitaxial mismatch, phase transformation, chemical reaction, moisture absorption, *etc*. In all these situations, the residual stresses can be considered to be equi-biaxial. As a result, Eq. (13) becomes

$$\begin{aligned}\varepsilon_x &= \frac{\partial u}{\partial x} + \frac{1}{2}\left(\frac{\partial w}{\partial x}\right)^2 + \frac{(1-\nu)\sigma^R}{E},\\ \varepsilon_y &= \frac{\partial v}{\partial y} + \frac{1}{2}\left(\frac{\partial w}{\partial y}\right)^2 + \frac{(1-v)\sigma^R}{E},\end{aligned} \tag{14}$$

and

$$\gamma_{xy} = \frac{\partial u}{\partial y} + \frac{\partial v}{\partial x} + \frac{\partial w}{\partial x}\frac{\partial w}{\partial y},$$

where we have taken $\sigma^R = \sigma_x^R = \sigma_y^R$. If the residual stresses are known, w_0, w_1, w_2, w_3, w_4 and u_0, v_0 can be determined as before. In the work of de Lumley-Woodyear [45], numerical solutions were developed based on the same energy method and using finite element software (ABAQUS®). However, the residual stresses were allowed to differ in the x and y directions. This led to a lack of uniqueness in the determination of the residual stresses. On the other hand, if they are the same in each direction, they can be uniquely extracted from the data. For the plane strain assumption (Appendix B), an exact solution can be obtained for the deflection w and in-plane displacement v:

$$w = \frac{qc^2}{2h\sigma_y}\left[1 - \left(\frac{y}{c}\right)^2\right] \tag{15a}$$

and

$$v = \frac{1-\nu^2}{E}(\sigma_y - \sigma^R)y - \frac{1}{6}\frac{q^2y^3}{(h\sigma_y)^2}, \tag{15b}$$

where

$$\begin{aligned}\sigma_y = \frac{1}{3}\sigma_c\Bigg(&\frac{\sigma^R}{\sigma_c} + \sqrt[3]{\frac{1}{2}\left(27 + 2\left(\frac{\sigma^R}{\sigma_c}\right)^3 + 3\sqrt{3}\sqrt{27 + 4\left(\frac{\sigma^R}{\sigma_c}\right)^3}\right)}\\ &+ \frac{(\sigma^R/\sigma_c)^2}{\sqrt[3]{1/2\left(27 + 2(\sigma^R/\sigma_c)^3 + 3\sqrt{3}\sqrt{27 + 4(\sigma^R/\sigma_c)^3}\right)}}\Bigg)\end{aligned} \tag{15c}$$

and

$$\sigma_c = \sqrt[3]{\frac{Eq^2c^2}{6h^2(1-v^2)}} \tag{15d}$$

is the stress under plane strain conditions.

In the present study, the residual stresses were caused by thermal contraction during curing. As a result, we assumed that the residual stress in x direction was the same as that in the y direction. Figure 10a shows the effects of the equi-biaxial residual stress on the maximum deflection of the membrane under constant uniform pressure. The quantities w_0, and σ_0 are, respectively, the maximum deflection and stress in the blister film in the absence of the residual stresses, and w_0' is the maximum deflection in the presence of residual stresses. Note that the equi-biaxial residual stress can be compressive and limited by the buckling stress in the film. In the present study, the specimen dimensions gave rise to a buckling stress of approximately $0.6\sigma_0$, establishing the lower limit of the abscissa in Figure 10a. It is clear that when the equi-biaxial residual stress is the same as σ_0, the maximum deflection decreases by 31%.

2.3. Energy Release Rate

Griffith [46] approached the fracture of an ideally brittle material from a thermodynamic point of view where the energy stored in a cracked body could be converted into surface energy as the crack grew. Irwin [47] developed the current version of this concept by introducing the energy release rate, G, which is defined as the rate of change in potential energy with crack area. Williams [27] discussed the link between fracture and adhesion in pressurized blister tests using a continuum interpretation. Our approach here is based on the energy release rate concept where

$$G\delta A = \delta W - \delta U - \delta D. \tag{16}$$

The quantity δA is the change of the debond area during crack propagation. The associated changes in the work done by the pressure, the strain energy in the blister, and the plastic and/or viscoelastic dissipation are, respectively, δW, δU, and δD. The possibility of viscoelastic dissipation is not considered here because the chosen materials were in their glassy state. Shirani and Liechti [38] showed that in the peninsula blister specimen, the amount of plastic dissipation was limited to a small region in the vicinity of the crack front, so this part can be

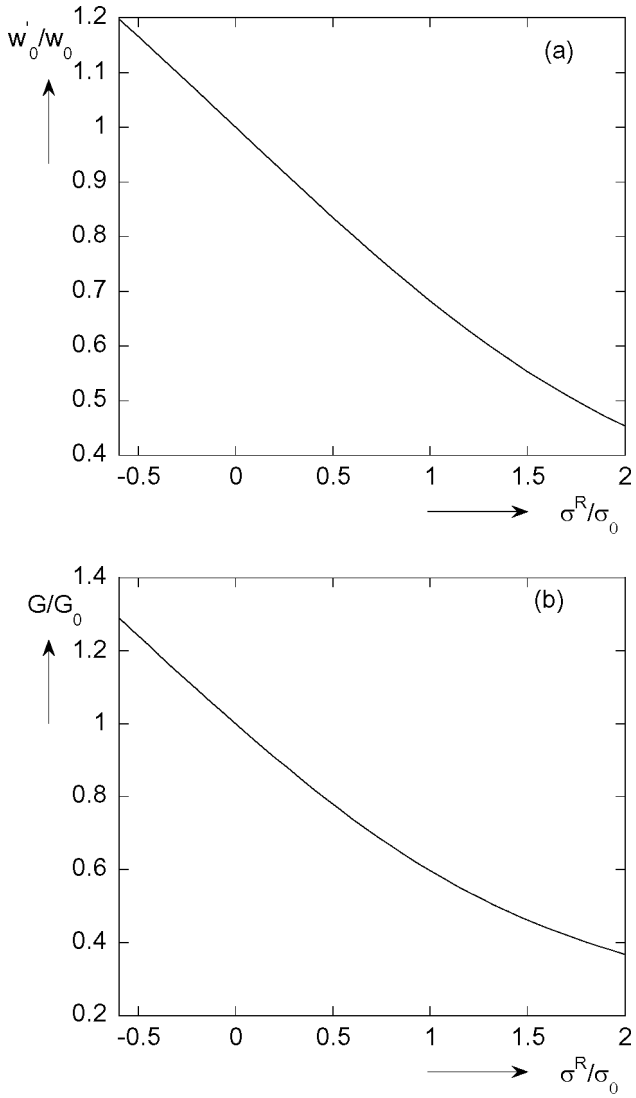

FIGURE 10 Effect of residual stress on (a) the maximum deflection and (b) the energy release rate.

neglected. Then, under these conditions, one can write

$$G\delta A = \delta W - \delta U. \tag{17}$$

Recalling the potential energy from Eq. (6), the expression of the

energy release rate is given by

$$G = -\frac{\partial \Pi}{\partial A} \tag{18}$$

For a peninsula blister specimen (Figure 1a), region 1 always satisfies the plane strain assumption ($a/c \geq 2$) whereas region 2 is, at least initially, a finite membrane. In spite of this, we verify that it is appropriate to determine the energy release rate based on the plane strain assumption even for $l_0/2c \geq 1.5$.

Based on the plane strain assumption ($\varepsilon_x = 0$), the strain energy per unit length of a membrane is given by

$$U' = \frac{Eh}{2(1-v^2)} \int_{-c}^{c} \varepsilon_y^2 dy, \tag{19}$$

where, from Appendix A,

$$\varepsilon_y = \sqrt[3]{\frac{(1-\nu^2)^2 q^2 c^2}{6h^2 E^2}}. \tag{20}$$

The external work per unit length is given by

$$W' = \int q w dy. \tag{21}$$

The total potential energy per unit length is obtained by

$$\pi = \frac{Eh}{2(1-\nu^2)} \int_{-c}^{c} \varepsilon_y^2 dy - \int_{-c}^{c} q w dy. \tag{22}$$

By substituting Eqs. (10a) and (21a) into Eq. (22) and letting $\nu = 0.3$,

$$\pi = -0.8804 \sqrt[3]{\frac{q^4 c^7}{Eh}}. \tag{23}$$

For region 1, by substituting

$$c = c - b/2 \tag{24}$$

into Eq. (23),

$$\pi_1 = -0.1746 \sqrt[3]{\frac{q^4 (c-b)^7}{Eh}}. \tag{25}$$

For region 2 based on the plane strain assumption,

$$\pi_2 = -0.8804 \sqrt[3]{\frac{q^4 c^7}{Eh}}. \tag{26}$$

In situations where region 2 is a membrane with a finite aspect ratio,

$$\Pi_2 = \frac{Eh}{2(1-\nu^2)} \int_{-a}^{a} \int_{-c}^{c} \left[\varepsilon_x^2 + \varepsilon_y^2 + 2\nu\varepsilon_x\varepsilon_y + \frac{1}{2}(1-\nu)\gamma_{xy}^2 \right] dx\, dy - \int_{-a}^{a} \int_{-c}^{c} qw\, dx\, dy \tag{27}$$

By substituting Eqs. (3) and (4a) into Eq. (27), the dimensionless total potential energy yields

$$\overline{\Pi}_2 = \frac{\Pi_2}{\sqrt[3]{q^4c^{10}/Eh}} = f_8\left(\nu, \frac{a}{c}\right). \tag{28}$$

From Eq. (26), the dimensionless potential energy for a plane strain membrane of length $2a$ is given by

$$\overline{\Pi}_p = \frac{\Pi_p}{\sqrt[3]{q^4c^{10}/Eh}} = \frac{2a\pi}{\sqrt[3]{q^4c^{10}/Eh}} = -1.7608\frac{a}{c}. \tag{29}$$

As a result, the dimensionless total potential energy in Eq. (28) should approach $-1.7608(a/c)$ for sufficiently long membranes.

Figure 11 shows the change of the dimensionless total potential energy, f_8, with aspect ratio, which can be approximated by $f_8 = 0.6678 - 1.7186(a/c)$ for $(a/c) > 1.5$. Comparing f_8 with the quantity $-1.7608(a/c)$ from the plane strain solution, it can be seen that, if the aspect ratio is larger than 1.5, the total potential energy calculated from the plane strain solution is accurate, and the deviation is less than 3%. As a result, in the following determination of the energy release rate, the total potential energy resulting from the plane strain solution for region 2 is appropriate for $l_0/2c \geq 1.5$.

The total potential energy of a specimen with the debond length, l, and the total length, L, is given by

$$\Pi = \pi_2 l + 2\pi_1(L-l). \tag{30}$$

The energy release rate is obtained by

$$G = -\frac{\partial\Pi}{\partial A} = -\frac{1}{2b}\frac{\partial\Pi}{\partial l} = \frac{1}{2b}(2\pi_1 - \pi_2) = \frac{1}{b}\sqrt[3]{\frac{q^4}{Eh}}\left[0.4402c^{7/3} - 0.1746(c-b)^{7/3}\right]. \tag{31}$$

In the geometry of our specimen, where $b = (1/8)c$, Eq. (31) simplifies to

$$G = 2.4987\sqrt[3]{\frac{q^4c^4}{Eh}}. \tag{32}$$

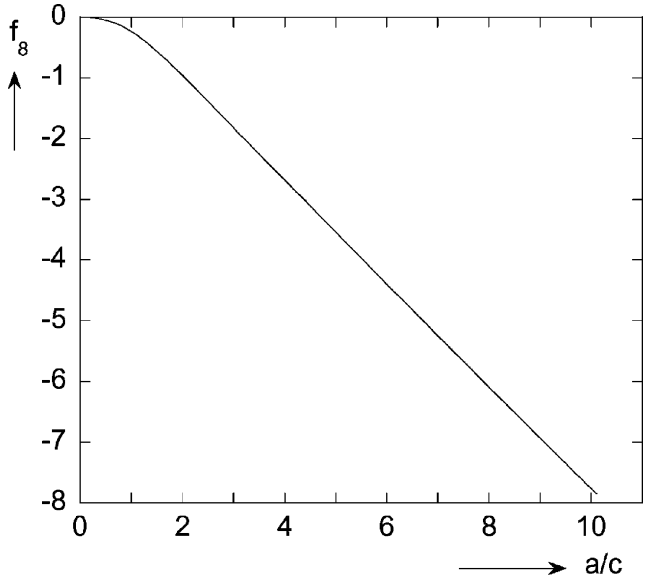

FIGURE 11 Variation of f_8 with aspect ratio ($\nu = 0.3$).

2.4. Effects of Residual Stresses for Energy Release Rate

We have shown how the residual stresses affect the deflection of a membrane. The effects of residual stresses on energy release rate in circular and island blister tests were considered in previous studies [32,48]. It was shown that the effects of residual stresses on energy release rate were significant. In the following, the effects of residual stresses on the energy release rate of the peninsula blister test are examined.

The strain energy in the membrane per unit length is given by

$$U' = \frac{Eh}{2(1-v^2)} \int_{-c}^{c} (\varepsilon_x^2 + \varepsilon_y^2 + 2\nu\varepsilon_x\varepsilon_y)\, dy \tag{33}$$

The total strains in the membrane are made up of the mechanical, ε^M, and residual strains, ε^R. For a plane strain membrane, this means that $\varepsilon_y = \varepsilon_y^M + \varepsilon^R$ and $\varepsilon_x = \varepsilon^R$. As a result, for a rectangular membrane with width $2c$ per unit length, Eq. (33) becomes

$$U' = \frac{Eh}{2(1-v^2)} \left[\int_{-c}^{c} 2(1+\nu)(\varepsilon^R)^2 dy + \int_{-c}^{c} 2(1+\nu)\varepsilon^R \varepsilon_y^M dy + \int_{-c}^{c} (\varepsilon_y^M)^2 dy \right]. \tag{34a}$$

The first integral in Eq. (34a) is the strain energy stored by the residual stresses. The second integral corresponds to the work done by the residual stresses through the displacements that occur during pressurization. The third integral is due to the work done by the membrane stresses acting through the displacement resulting from the pressure. In preparation for considering the potential energy due to the pressure, the net strain energy per unit length is

$$U' = \frac{Eh}{2(1-v^2)}\left[\int_{-c}^{c} 2(1+\nu)\varepsilon^R \varepsilon_y^M dy + \int_{-c}^{c} (\varepsilon_y^M)^2 dy\right]. \tag{34b}$$

The total potential energy of a membrane per unit length is obtained from

$$\pi = \frac{Eh}{2(1-v^2)}\left[\int_{-c}^{c} 2(1+\nu)\varepsilon^R \varepsilon_y^M dy + \int_{-c}^{c} (\varepsilon_y^M)^2 dy\right] - \int_{-c}^{c} qw\, dy \tag{34c}$$

This result is derived under the tacit assumption that the strain energy in the substrate is neglected because the substrate is much stiffer than the film.

For a sufficiently long region 2 in a peninsula blister specimen, the deflection and in-plane strain are given by (Appendix B)

$$w = \frac{qc^2}{2h\sigma_{y1}}\left[1 - \left(\frac{y}{c}\right)^2\right], \tag{35a}$$

$$\varepsilon_y^M = \frac{1-\nu^2}{E}(\sigma_{y2} - \sigma^R) \tag{35b}$$

and

$$\varepsilon^R = \frac{(1-\nu)\sigma^R}{E}, \tag{35c}$$

where $\sigma_{c2} = \sqrt[3]{Eq^2c^2/6h^2(1-v^2)}$ and

$$\sigma_{y2} = \frac{1}{3}\sigma_{c2}\left(\frac{\sigma^R}{\sigma_{c2}} + \sqrt[3]{\frac{1}{2}\left[27 + 2\left(\frac{\sigma^R}{\sigma_{c2}}\right)^3 + 3\sqrt{3}\sqrt{27 + 4\left(\frac{\sigma^R}{\sigma_{c2}}\right)^3}\right]} + \frac{(\sigma^R/\sigma_{c2})^2}{\sqrt[3]{1/2\left(27 + 2(\sigma^R/\sigma_{c2})^3 + 3\sqrt{3}\sqrt{27 + 4(\sigma^R/\sigma_{c2})^3}\right)}}\right).$$

Substituting Eqs. (35a, b, and c) into Eq. (34c), the total potential energy per unit length for region 2 is

$$\pi_2 = \frac{(1-\nu^2)hc}{2E}\left[\sigma_{y2}^2 - (\sigma^R)^2\right] - \frac{2q^2c^3}{3h\sigma_{y2}}. \tag{35d}$$

For region 1, the membrane stress in y direction is given by

$$\sigma_{y1} = \frac{1}{3}\sigma_{c1}\left(\frac{\sigma^R}{\sigma_{c1}} + \sqrt[3]{\frac{1}{2}\left[27 + 2\left(\frac{\sigma^R}{\sigma_{c1}}\right)^3 + 3\sqrt{3}\sqrt{27 + 4\left(\frac{\sigma^R}{\sigma_{c1}}\right)^3}\right]} + \frac{(\sigma^R/\sigma_{c1})^2}{\sqrt[3]{1/2\left(27 + 2(\sigma^R/\sigma_{c1})^3 + 3\sqrt{3}\sqrt{27 + 4(\sigma^R/\sigma_{c1})^3}\right)}}\right), \tag{36a}$$

where

$$\sigma_{c1} = \sqrt[3]{\frac{Eq^2}{6h^2(1-v^2)}\left(\frac{c-b}{2}\right)^2}. \tag{36b}$$

In our case, $b = c/8$, and then Eq. (35b) becomes

$$\sigma_{c1} = \sqrt[3]{\frac{49}{256}}\sqrt[3]{\frac{Eq^2c^2}{6h^2(1-v^2)}} = \sqrt[3]{\frac{49}{256}}\sigma_{c2}. \tag{36c}$$

By substituting Eq. (36c) into Eq. (36a), the membrane stress in region 1 becomes

$$\sigma_{y1} = \frac{1}{3}\sqrt[3]{\frac{49}{256}} \times \sigma_{c2}\left(\sqrt[3]{\frac{256}{49}}\frac{\sigma^R}{\sigma_{c2}} + \sqrt[3]{\frac{1}{2}\left[27 + \frac{512}{49}\left(\frac{\sigma^R}{\sigma_{c2}}\right)^3 + 3\sqrt{3}\sqrt{27 + \frac{1024}{49}\left(\frac{\sigma^R}{\sigma_{c2}}\right)^3}\right]} + \frac{\sqrt[3]{(256/49)^2}(\sigma^R/\sigma_{c2})^2}{\sqrt[3]{1/2\left(27 + 512/49(\sigma^R/\sigma_{c2})^3 + 3\sqrt{3}\sqrt{27 + 1024/49(\sigma^R/\sigma_{c2})^3}\right)}}\right). \tag{36d}$$

Finally the deflection and in-plane strain for region 1 are obtained from

$$w = \frac{49qc^2}{512h\sigma_{y1}}\left[1 - \frac{256}{49}\left(\frac{y}{c}\right)^2\right], \tag{36e}$$

$$\varepsilon_y^M = \frac{1-\nu^2}{E}(\sigma_{y1} - \sigma^R), \tag{36f}$$

and

$$\varepsilon^R = \frac{(1-\nu)\sigma^R}{E}. \tag{36g}$$

Substituting Eqs. (36e, f and g) into Eq. (34c) yields the total potential energy per unit length for region 1:

$$\pi_1 = \frac{7(1-\nu^2)hc}{32E}\left[\sigma_{y1}^2 - (\sigma^R)^2\right] - \frac{343q^2c^3}{6144h\sigma_{y1}}. \tag{36h}$$

By substituting Eqs. (35d) and (36h) into Eq. (31), the energy release rate is obtained from

$$G = \frac{1}{2b}(2\pi_1 - \pi_2) = \left(\frac{8}{3\sigma_{y2}} - \frac{343}{768\sigma_{y1}}\right)\frac{q^2c^2}{h} + \left[\left(\frac{7\sigma_{y1}^2}{4} - 2\sigma_{y2}^2\right) + \frac{1}{4}(\sigma^R)^2\right]\frac{(1-\nu^2)h}{E}. \tag{37}$$

Figure 10b shows the effect of the equi-biaxial residual stress on the energy release rate under the assumption of a constant pressure. The quantities G_0 and σ_0 are, respectively, the energy release rate and stress in the blister film in the absence of the residual stresses. It is clear (Figure 10b) that the energy release rate depends strongly on the residual stress state. If compressive residual stresses are present, the energy release rate is underestimated if they are neglected, and *vice versa* for tensile residual stresses. When the residual stress is of the same order as the stress resulting from the uniform pressure, the energy release rate is overestimated by 40%. From the point of view of an energy balance, the pressure drives the delamination as well as overcoming the residual stresses. In other words, for the same interface, the critical pressure for initiating debonding with tensile

TABLE 2 Dimensions and Properties of the Specimen

Property	Value
2c	10.16 mm
2b	1.27 mm
$l_0/2c$	1.5
h	127 μm
E	1.78 GPa
ν	0.30
σ^R	5.70 MPa

residual stresses will be higher than that without any residual stresses. In reality, there are very few film–substrate systems without residual stresses. As a result, when the energy release rate needs to be determined, the residual stresses also need to be considered.

4. RESULTS AND DISCUSSION

In this section, the results from the experimental and analytical procedures that were developed in the forgoing sections are presented and compared. First, the blister shape for the analytical solution and a finite element analysis were checked against the measurements. The energy release rate was then determined based on the analytical solution and compared with energy release rate solutions from other sources. The mechanical properties and dimensions of the specimen are summarized in Table 2.

4.1. Blister Shape

The shape of the blistered film played a key role in determining the energy release rate. The foregoing analytical solution, which has a limited number of degrees of freedom, was checked against both experimental data and the solution of a finite element analysis. A finite element model consisting of 1500 S4 elements was developed using ABAQUS.[2] This element type is a four-node doubly curved, general purpose, finite-membrane-strain shell element, which has four integration points [49] and can be used effectively where in-plane bending is expected.

Figure 12 compares the deflected shape in the *yz* and *xz* planes from the bulge test with the results from the analytical and finite element

[2]The authors acknowledge the use of the finite element package ABAQUS® under academic license.

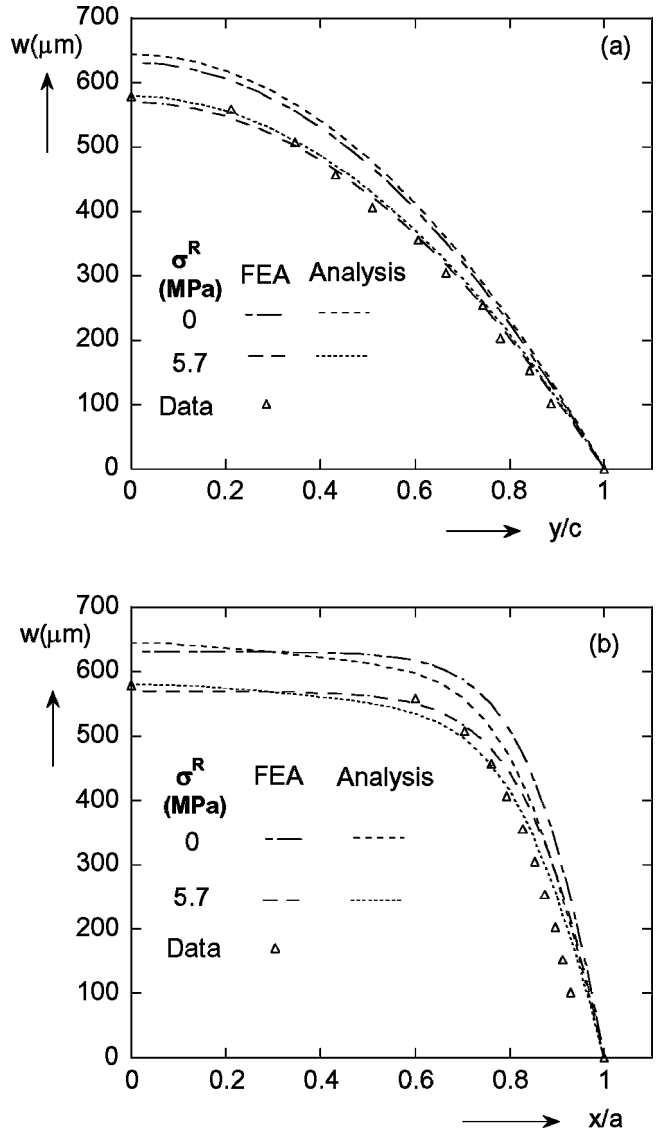

FIGURE 12 Membrane shape in (a) the yz plane and in (b) the xz plane for a pressure of 121.9 kPa in a specimen with Hysol EA 9696 bonded to Al 6061-T6.

analyses. As was mentioned earlier, the residual stresses had about a 10% effect on the central deflection. In the *yz* plane, the shape of the membrane was the same for both the analyses (Figure 12a). There was

a slight difference between the measurements and the analyses for $x/c \geq 0.8$, where there is probably a boundary layer effect [50,51]. The deflections from the analyses did differ by as much as 2% in the xz plane. This was because in the analytical solution, a limited number of terms was used to represent the deflection in the x direction, making it slightly stiffer than the finite element result. The difference between the measurements and finite analysis in the region $x/a \geq 0.7$ (Figure 12b) was more noticeable than in Figure 12a.

The deflection during delamination was obtained by taking a profile (Figure 13) of the shadow moiré fringes along the centerline of the peninsula. This procedure traced the deflected shapes of the peninsula blister in region 2 as the delamination advanced and corresponds to the pressure and debond histories that are shown in Figure 5. When the delamination length was such that $l/2c \geq 1.7$ $(t \geq 1320\text{s})$, the maximum deflection of the blister appeared to remain constant. However, if the fringe data had been interpolated, it is likely that the central displacements increased with crack length and time as indicated by the analysis. It is interesting to note that the measured deflections were again consistently lower than the values obtained from the analytical solution in the region near the delamination front. The pressure

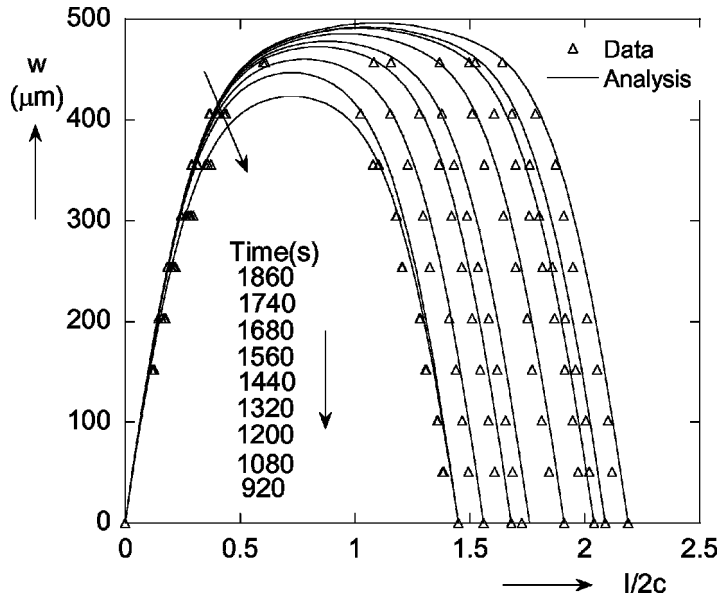

FIGURE 13 Comparison of measured crack profiles with solutions from the approximate analysis in a specimen with Hysol EA 9696 bonded to Al 6061-T6.

levels in the peninsula blister specimen were lower than those that were applied in the bulge test with the result that the boundary layer would be more extensive.

4.2. Interfacial Toughness

The energy release rates determined from the plane strain analysis, the analytical solution based on the minimization of energy, and the finite element analysis of the blister specimen are shown in Table 3. These values were obtained for the steady state delamination pressure of $86.6 \pm 1\%$ kPa with $\sigma^R = 0$ or $\sigma^R = 5.70\,\text{MPa}$. The values in the plane strain column were determined using Eqs. (32) and (37), respectively. The values in the analytical column were determined by assuming that region 2 is a finite membrane. Recall that the plane strain assumption was valid if $l/2c \geq 1.5$. The third column gives the results from the finite element analysis where the difference in potential energy at two different crack lengths was divided by the change in crack surface area. These values were all compared with Dillard and Bao's results [34] based on a membrane assumption that the deflection was a circular arc. Because the maximum deflection was considerably smaller than the width of the specimen, the circular arc turned out to be a good approximation of the true deflected shape. As a result, the values of the energy release rate were quite similar at zero residual stress. However, an examination of the results in the row corresponding to $\sigma^R = 5.70\,\text{MPa}$ indicates that the assumption [34] that the residual stresses were dominant was not reasonable. First, the stress level due to pressurization was about 15 MPa, three times as large as the residual stress. Second, a tensile residual stress should decrease rather than increase the energy release rate ([47] and Figure 10b). This discrepancy is due to the manner in which the membrane stress was handled in Ref. [34]. The reason for the $5\,\text{J/m}^2$ difference between the plane strain and analytical energy release rate values was due to

TABLE 3 Comparison of the Interfacial Toughness Values (J/m^2) for Hysol EA 9696/Alumimum 6069-T6

Residual stress (MPa)	Plane strain (J/m^2)	Analytical (J/m^2)	Finite element (J/m^2)	Dillard & Bao (J/m^2)
0	137	134	135	139
5.70	113	108	107	297

Note. Toughness values are given to within $\pm 2\%$.

the fact that the analytical solution includes a biaxial rather than uniaxial residual stress state. The levels of toughness encountered here are about one third of the values obtained by Moidu *et al*. [52] in a peel test of Hysol EA 9346 from aluminum that had yet to be exposed to water. This difference may be due to the fact that the plastic dissipation in the peninsula blister test is minimized. It was shown in a cohesive zone analysis that accounted for the elasto-plastic behavior of the film [39] that the amount of plastic dissipation was limited to a small region of the vicinity of the crack front, and was 6% of the adhesive fracture energy. The lower values were unlikely to be due to the presence of the pressurizing fluid, which was in contact with the bond for only 2 h, which is insufficient for significant diffusion.

5. CONCLUSIONS

A stress and fracture analysis of the peninsula blister test has been presented. The analysis accounted for large deformations of the blistering film and residual stresses in it. An analytical solution based on a fully clamped rectangular membrane and the minimum potential energy method was developed to predict the deflection in each inflated region of the specimen. A finite element solution was also developed, mainly for validation purposes. There was good agreement between both the analytical and finite element solutions and the measured blister shape.

Relatively simple expressions for the energy release rate were developed for cracks that were longer than 1.5 times the specimen width. Under this condition, the energy release rate is independent of crack length. In the absence of residual stresses, users are referred to Eq. (31) for the energy release rate. On the other hand, when residual stresses are important, Eq. (37) combined with appropriate elements of Eqs. (35) and (36) should be used. Toughness values obtained from these expressions should be very close to the intrinsic toughness of the interface because of the relatively small amounts of plastic dissipation that occur in this specimen.

An attractive feature of the peninsula blister test is that it can be turned into a bulge test following complete delamination along the peninsula. This allows the Young's modulus of, and the residual stresses in, the delaminated film to be determined from the pressure–volume response. For the Hysol EA 9696 film adhesive that was used in this study, the Young's modulus and residual stresses were 1.78 GPa and 5.7 MPa, respectively.

The peninsula blister tests that were conducted in the current study produced steady-state crack growth, and debonding took place at a

constant pressure with a minimal amount of plastic dissipation. The toughness of the Hysol EA 9696/aluminum interface, accounting for residual stresses, was $108 \pm 2\,\mathrm{J/m^2}$.

Thus, the peninsula blister configuration is very suitable for measuring the adhesive fracture energy of thin films. The effect of aggressive environments or solvents can easily be incorporated in a contained and convenient manner when they are used as the pressurizing fluid. For specimens with brittle films and/or interfaces with very high toughness values, the film may burst, but this problem can easily be rectified by reinforcing the film with a suitable coating.

APPENDIX A: THE PLANE STRAIN DEFLECTION OF A THIN MEMBRANE

Considering the large deflection of a plate with a bending stiffness, D, the equilibrium equation can be expressed [43] in terms of the deflection, w, and the forces per unit length, N_x, N_y, N_{xy}, as

$$D\nabla^4 w = q + N_x \frac{\partial^2 w}{\partial^2 x} + N_y \frac{\partial^2 w}{\partial^2 y} + 2N_{xy} \frac{\partial^2 w}{\partial x \partial y}. \tag{A1}$$

If the deflection is much greater than the plate thickness, h, a thin membrane can be assumed, making $D = 0$. In addition, if the membrane is infinitely long in the x direction, plane strain applies, and (A1) can be simplified to

$$\frac{\partial^2 w}{\partial^2 y} = -\frac{q}{N_y} = -\frac{q}{h\sigma_y}. \tag{A2}$$

In addition, $d\sigma_y/dy = 0$, $w = f(y)$, and the in-plane y displacement, v, is

$$v = g(y). \tag{A3}$$

The boundary conditions are

$$w(\pm c) = 0, \tag{A4a}$$

$$w'(0) = 0, \tag{A4b}$$

$$v(\pm c) = 0 \tag{A4c}$$

and

$$v(0) = 0. \tag{A4d}$$

The strain displacement equation is

$$\varepsilon_y = \frac{dv}{dy} + \frac{1}{2}\left(\frac{\partial w}{\partial y}\right)^2. \tag{A5}$$

The linearly elastic and isotropic membrane has the stress-strain behavior

$$\sigma_y = \frac{E}{1-\nu^2}\varepsilon_y. \tag{A6}$$

Noting that σ_y is constant (but unknown) and integrating Eq. (A2) with boundary conditions (A4a) and (A4b) yields the deflection

$$w = \frac{q}{2h\sigma_y}(c^2 - y^2). \tag{A7}$$

Substituting Eq. (A7) into Eq. (A5) and integrating subject to Eq. (A4d) gives the displacement

$$v = \frac{1-\nu^2}{E}\sigma_y y - \frac{1}{6}\frac{q^2 y^3}{(h\sigma_y)^2}. \tag{A8}$$

Finally, the boundary condition (A4c) gives us the membrane stress

$$\sigma_y = \sqrt[3]{\frac{Eq^2c^2}{6h^2(1-\nu^2)}}. \tag{A9}$$

The expression for the stress can now be substituted into Eq. (A7) for the deflection, so that

$$w = \sqrt[3]{\frac{6q(1-\nu^2)}{8hEc^2}}(c^2 - y^2). \tag{A10}$$

Similarly, by substituting the stress into Eq. (A8), we obtain the displacement

$$v = \sqrt[3]{\frac{(1-\nu^2)^2 q^2 c^2}{6h^2E^2}}\, y - \sqrt[3]{\frac{(1-\nu^2)^2 q^2}{6h^2E^2c^4}}\, y^3. \tag{A11}$$

Substituting the stress into Eq. (A6) yields the strain

$$\varepsilon_y = \sqrt[3]{\frac{(1-\nu^2)^2 q^2 c^2}{6h^2E^2}}. \tag{A12}$$

APPENDIX B: THE DEFLECTION OF A THIN MEMBRANE WITH RESIDUAL STRESS

The in-plane displacement and deflection are measured from the beginning of pressurization rather than from the initial state. Thus Eqs. (A5) and (A6) become

$$\varepsilon_y = \frac{dv}{dy} + \frac{1}{2}\left(\frac{\partial w}{\partial y}\right)^2 = \frac{1-\nu^2}{E}(\sigma_y - \sigma^R), \tag{B1}$$

where σ^R is the equibiaxial residual stress.
Equation (A8) becomes

$$v = \frac{1-\nu^2}{E}(\sigma_y - \sigma^R)y - \frac{1}{6}\frac{q^2y^3}{(h\sigma_y)^2}, \tag{B2}$$

and enforcing (A4c) now yields

$$\sigma_y^3 - \sigma^R\sigma_y^2 = \frac{Eq^2c^2}{6h^2(1-v^2)} = A, \tag{B3}$$

whose solution is

$$\sigma_y = \frac{1}{3}\left(\sigma^R + \sqrt[3]{1/2(27A + 2\sigma^{R^3} + 3\sqrt{3}\sqrt{27A^2 + 4A\sigma^{R^3}})}. \right.$$
$$\left. + \frac{\sigma^{R^2}}{\sqrt[3]{1/2(27A + 2\sigma^{R^3} + 3\sqrt{3}\sqrt{27A^2 + 4A\sigma^{R^3}})}}\right). \tag{B4}$$

Substituting the stress into Eqs. (A7), (B2), and (B1) gives the deflection, in-plane displacement, and strain with the residual stress effect. In particular, we see that the central deflection is

$$w_0 = \frac{qc^2}{2h\sigma_y}, \tag{B5}$$

and the pressure-central deflection response is then

$$q = \frac{2h\sigma^R}{c^2}w_0 + \frac{8Eh}{6c^4(1-\nu^2)}w_0^3. \tag{B6}$$

ACKNOWLEDGMENTS

Two of the authors (K. M. L., T. L. W.) thank Hewlett-Packard Company (HP) for its financial support of this project in its early phases. In addition, Brad Benson (HP) provided generous technical support.

REFERENCES

[1] Liechti, K. M. and Shirani, A., *Int. J. Fracture* **67**, 21–36 (1994).
[2] Langier, M. T., *Thin Solid Films* **117**, 243–249 (1984).
[3] Wu, T. W., *J. Mater. Res.* **6**, 407–426 (1991).
[4] Venkataraman, S., Kohlstedt, D. L., and Gerberich, W. W., *J. Mater. Res.* **11**, 3133–3145 (1996).
[5] Thouless, M. D., *Eng. Fracture Mech.* **61**, 75–81 (1998).
[6] Chapman, B. N., *J. Vac. Sci. Technol.* **11**, 106–113 (1974).
[7] Baglin, J. E. and Clark, G. J., *Nucl. Instrum. Meth. B7* **8**, 881–885 (1985).
[8] Jacobsen, R., *Thin Solid Films* **34**, 191–199 (1976).
[9] Dauskardt, R. H., Lane, M., Ma, Q., and Krishna, N., *Eng. Fract. Mech.* **61**, 141–162 (1998).
[10] Bagchi, A., Lucas, G. E., Suo, Z., and Evans, A. G., *J. Mater. Res.* **9**, 1734–1741 (1994).
[11] Bagchi, A. and Evans, A. G., *Thin Solid Films* **286**, 230–212 (1996).
[12] Marshall, D. B. and Evans, A. G., *J. Appl. Phys.* **10**, 2632–2638 (1984).
[13] Rosenfeld, L. G., Ritter, J. E., Lardner, T. J., and Lin, M. R., *J. Appl. Phys.* **67**, 3291–3296 (1990).
[14] DeBoer, M. P. and Gerberich, W. W., *Acta Mater.* **33**, 3169–3175 (1996).
[15] Kriese, M. D., Gerberich, W. W., and Moody, N. R., *J. Mater. Res.* **14**, 3007–3018 (1999).
[16] Kriese, M. D., Gerberich, W. W., and Moody, N. R., *J. Mater. Res.* **14**, 3019–3026 (1999).
[17] Cordill, M. J., Bahr, D. F., Moody, N. R., and Gerberich W. W., *Device and materials Reliability* **4**, 163–167 (2004).
[18] Gent, A. N. and Hamed, G. R., *J. Adhes.* **7**, 91–95 (1975).
[19] Nicholson, D. W., *Int. J. Fracture* **13**, 279–287 (1977).
[20] Kim, J., Kim, K. S. and Kim, Y. H., *J. Adhes. Sci. Tech.* **3**, 175–187 (1989).
[21] Kinloch, A. J., Dukes, W. A., and Gledhill, R. A., *J. Adhes. Sci. Tech.* **2**, 597–614 (1975).
[22] Wei, Y. and Hutchinson, J. W., *J. Mech. Phys. Solids* **45**, 1253–1273 (1997).
[23] Kim, K.-S. and Aravas, N., *Int. J. Solids Structures* **24**, 417–435 (1988).
[24] Dannenberg, H., *J. Appl. Polymer Sci.* **5**, 125–134 (1961).
[25] Malyshev, B. M. and Salganik, R. L., *Int. J. Fracture* **36**, 199–217 (1965).
[26] O'Brien, E. P., Ward, T. C., Guo, S., and Dillard, D. A., *J. Adhes.* **79**, 69–97 (2003).
[27] Williams, M. L., *J. Appl. Polymer Sci.* **13**, 29–40 (1969).
[28] Hinkley, J. A., *J. Adhes.* **16**, 115–125 (1983).
[29] Gent, A. N. and Lewandowski, L. H., *J. Appl. Polymer Sci.* **33**, 1567–1577 (1987).
[30] Wan, K. T. and Breach, C., *J. Adhes.* **66**, 182–201 (1998).
[31] Wan, K. T., *Int. J. Adhes. Adhesives* **20**, 141–143 (2000).
[32] Allen, M. G. and Senturia, S. D., *J. Adhes.* **25**, 303–315 (1988).
[33] Chang, Y. S., Lai, Y. H., and Dillard, D. A., *J. Adhes.*, **27**, 197–211 (1989).
[34] Lai, Y. H. and Dillard, D. A., *J. Adhes.* **31**, 177–189 (1990).
[35] Allen, M. G. and Senturia, S. D., *J. Adhes.* **29**, 219–231 (1989).
[36] Dillard, D. A. and Bao, Y., *J. Adhes.* **22**, 253–272 (1991).
[37] Lai, Y. H. and Dillard, D. A., *J. Adhes. Sci. Tech.* **8**, 663–678 (1994).
[38] Shirani, A. and Liechti, K. M., *Int. J. Fracture* **93**, 281–314 (1998).
[39] Needleman, A., *J. Appl. Mech.* **54**, 525–531 (1987).
[40] Needleman, A., *J. Mech. Phys. Solids* **38**, 289–324 (1990).

[41] Shirani, A. in *Aerospace Engineering and Engineering Mechanics* (University of Texas at Austin, Austin, 1997).
[42] Vlasssak, J. J. and Nix, W. D., *J. Mater. Res.* **7**, 3242–3249 (1992).
[43] Timoshenko, S. P. and Woinowsky-Krieger, S., *Theory of Plates and Shells* (McGraw-Hill, New York, 1987).
[44] Allen, M. G., Mehregany, M., Howe, R. T., and Senturia, S. D., *Appl. Phys. Lett.* **51**, 241–243 (1987).
[45] De Lumley-Woodyear, T. H., in *Research Center for the Mechanics of Solids, Structures & Materials Report CSSM-01/8* (University of Texas at Austin, Austin, 2001).
[46] Griffith, A. A., *Philos. Trans. R. Soc. London A* **19**, 897–908 (1915).
[47] Irwin, G. R. Sagamore Research Conference Procedings (New York, 1956), pp. 289–305.
[48] Jensen, H. M. and Thouless, M. D., *Int. J. Solids Structures* **30**, 779–795 (1993).
[49] Hibbitt, Karlsson and Sorensen, *ABAQUS Standard Users's Manual, Version 6.1.* (Hibbitt, Karlsson and Sorensen, Inc., Providence, RI, 2000).
[50] Gioia, G. and Ortiz, M., *Adv. Appl. Mech.* **33**, 119–192 (1997).
[51] Jensen, H. M., *Int. J. Fracture* **94**, 79–88 (1998).
[52] Moidu, A. K., Sinclair, A. N., and Spelt, J. K., *J. Adhes.* **65**, 239–257 (1998).